nature geoscience

ARTICLES

https://doi.org/10.1038/s41561-021-00697-1

Multi-decadal trends in Antarctic sea-ice extent driven by ENSO–SAM over the last 2,000 years

Xavier Crosta[1]✉, Johan Etourneau[1,2], Lisa C. Orme[3], Quentin Dalaiden[4], Philippine Campagne[1], Didier Swingedouw[1], Hugues Goosse[4], Guillaume Massé[5], Arto Miettinen[6,11], Robert M. McKay[7], Robert B. Dunbar[8], Carlota Escutia[9] and Minoru Ikehara[10]

Antarctic sea ice has paradoxically become more extensive over the past four decades despite a warming climate. The regional expression of this trend has been linked to changes in vertical redistribution of ocean heat and large-scale wind-field shifts. However, the short length of modern observations has hindered attempts to attribute this trend to anthropogenic forcing or natural variability. Here, we present two new decadal-resolution records of sea ice and sea surface temperatures that document pervasive regional climate heterogeneity in Indian Antarctic sea-ice cover over the last 2,000 years. Data assimilation of our marine records in a climate model suggests that the reconstructed dichotomous regional conditions were driven by the multi-decadal variability of the El Niño Southern Oscillation and Southern Annular Mode (SAM). For example, during an El Niño/SAM– combination, the northward sea-ice transport was reduced while heat advection from the subtropics to the Southern Ocean increased, which resulted in reduced sea-ice extent in the Indian sector as sea ice was compacted along the Antarctic coast. Our results therefore indicate that natural variability is large in the Southern Ocean and suggest that it has played a crucial role in the recent sea-ice trends and their decadal variability in this region.

The annual cycle of Antarctic sea ice, oscillating from a mean winter extent of ~18.5×10^6 km^2 to a mean summer extent of ~3.1×10^6 km^2, exerts a strong control on Southern Ocean (SO) circulation and its ecosystems[1], as well as on global climate via the modulation of atmospheric CO_2 concentrations and global ocean circulation[2]. Since the beginning of satellite measurements in 1979, total Antarctic sea-ice extent has increased by ~1.5% per decade[3]. However, there have been marked regional differences, including sea-ice decreases in the Amundsen–Bellinghausen sector and increases in the western Pacific and Atlantic sectors[4]. Because the satellite record is very short (<41 years), the processes underlying this regional heterogeneity, such as changes in wind-induced ice drift[1,5] and in ocean heat vertical redistribution[6], are still debated. The relative importance of natural variability and human-induced activities (mainly anthropogenic greenhouse gas emissions and ozone hole) in driving these sea-ice changes is currently unknown. In particular, our knowledge of SO natural variability[7] is limited due to the lack of records of its past evolution. Furthermore, most of the current coupled climate models are not able to reproduce the monitored increase in Antarctic sea ice[8], which may severely hamper any robust projections of Antarctic sea-ice evolution and associated oceanographic and climatic feedbacks over the coming decades. Acquisition of decadal-scale Antarctic sea-ice records is therefore crucial to improve our understanding of the natural patterns and drivers of sea-ice variability as a basis to explain the recent observed trends.

Only a few records of Holocene Antarctic sea-ice dynamics exist, and these are generally at multi-centennial resolution[9–12]. Therefore, none of these records allows for a robust understanding of the processes driving multi-decadal sea-ice variability. In this article, we describe sea-ice dynamics in the Indian sector of the SO over the last 2,000 years and identify potential drivers through comparison with published palaeoclimate records and offline data assimilation (DA) using Community Earth System Model version 1 Community Atmospheric Model version 5 (CESM1-CAM5 coupled ocean–atmosphere General Circulation Model). We analysed diatom assemblages and diatom-specific biomarkers in a 40-m-long sediment sequence at Integrated Ocean Drilling Program (IODP) U1357B Hole (66° 25' S, 140° 26' E, 1,026 m water depth) recovered on the Adélie Land coast (ALC) continental shelf to reconstruct sea-ice duration off East Antarctica over the 0–1900 CE period at a sub-decadal resolution. Concomitantly, we analysed diatom assemblages in a 0.5 m sediment sequence at COR1GC site (54° 16' S, 39° 46' E, 2834 m of water depth) from the Indian Antarctic Polar Front (APF) to reconstruct summer sea surface temperatures (SSTs) in the open ocean zone of the Indian sector over the 0–1000 CE period at a multi-decadal resolution (Fig. 1). Core descriptions and chronologies can be found in refs. [13,14], respectively, and in the Methods.

Environmental conditions inferred from marine records

Sea-ice-related diatoms (*Fragilaropsis curta* and *F. cylindrus*; ref. [15]) and highly branched isoprenoids (HBIs, ratio of diene to triene; ref. [16]) preserved in marine sediment records are commonly used to infer past changes in spring sea-ice conditions, with high values of

[1]Université de Bordeaux, CNRS, EPHE, UMR 5805 EPOC, Pessac, France. [2]EPHE-PSL Research University, Paris, France. [3]ICARUS, Department of Geography, Maynooth University, Maynooth, Ireland. [4]Earth and Life Institute (ELI), Université catholique de Louvain (UCL), Louvain-La-Neuve, Belgium. [5]LOCEAN, UMR CNRS/UPCM/IRD/MNHN 7159, Université Pierre et Marie Curie, Paris, France. [6]Norwegian Polar Institute, Tromsø, Norway. [7]Antarctic Research Centre, Victoria University of Wellington, Wellington, New Zealand. [8]School of Earth, Energy, and Environmental Sciences, Stanford University, Stanford, CA, USA. [9]Andaluz Institute of Earth Sciences, CSIC-University of Granada, Granada, Spain. [10]Center for Advanced Marine Core Research, Kochi University, Nankoku, Japan. [11]Present address: Ecosystems and Environment Research Programme, University of Helsinki, Helsinki, Finland. ✉e-mail: xavier.crosta@u-bordeaux.fr

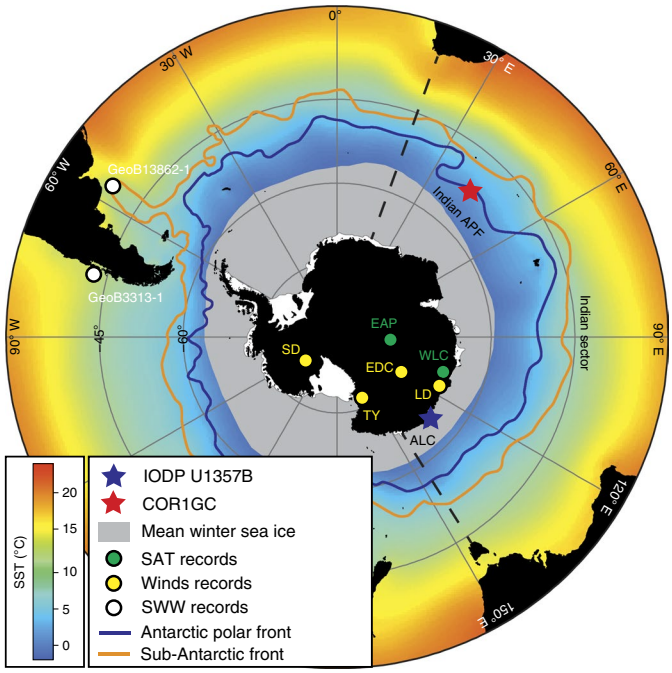

Fig. 1 | Location of studied marine cores and modern SO hydrographic features. IODP Hole U1357B site is shown by the blue star and COR1GC by the red star. The background map represents the modern (1955–2008) mean annual SST field from the World Ocean Atlas 2009 (https://www.nodc.noaa.gov; ref. [45]). The modern mean locations of the sub-Antarctic Front (orange line) and APF (blue line) are from ref. [46]. The modern mean winter sea-ice extent (grey shaded area) is from ref. [47]. Green dots indicate the locations of the composite SAT reconstruction for the East Antarctic Plateau region (EAP) and the Wilkes Land coast area (WLC)[19]. Yellow dots show the locations of wind records reconstructed from the sodium records in Law Dome (LD), EPICA Dome C (EDC), Taylor Dome (TY) and Siple Dome (SD)[24]. White dots identify the locations of the westerly winds reconstructions inferred from the iron content in core GeoB3313-1 (ref. [22]) and from ice-volume-corrected *Globorotalia inflata* $\delta^{18}O$ values in core GeoB13862-1 (ref. [23]). The delineation of the Indian Ocean is from ref. [48].

either proxy indicating persistent sea ice (Methods). Relative abundances of the *F. curta* group (Fig. 2b) show two periods of higher values at −200 to 500 CE (Period 1) and 830–1520 CE (Period 3), indicating a late-spring sea-ice retreat in ALC. Two periods of lower abundances at 500–830 CE (Period 2) and 1520–1850 CE (Period 4) conversely suggest early-spring sea-ice retreat. On the basis of the *F. curta* group record, the most recent period at 1850–1900 CE probably had late-spring sea-ice retreat. The diene/triene values (Fig. 2a) were generally higher during Periods 1 and 3 than during Period 2. Diene/triene values were generally low during Period 4, except for two short-lived events that are in phase with small increases in the *F. curta* group. When comparing these records with the *Thalassiosira antarctica* record, a diatom species whose high abundances are commonly used to infer early sea-ice return in autumn[17] (Methods), we find a different seasonal evolution of spring and autumn sea-ice conditions over the last 2,000 years. Indeed, average relative abundances of *T. antarctica* are observed during Periods 1 and 3 (Fig. 2c), while low abundances characterized Period 2, suggesting late sea-ice formation compared with Periods 1 and 3. Conversely, much higher abundances persisted throughout Period 4, indicating that this time saw the earliest sea-ice return of the last 2,000 years. The comparison of these data with diatom distributions in modern SO sediments[18] and in ALC sediments covering the instrumental period[15] allows us to estimate regional sea-ice duration (Extended Data Fig. 1). This suggests sea-ice presence (SIP) of 8–9 months per year during Period 1 (late melting, early freezing), 7–8 months per year during Period 2 (early melting, late freezing), 9–10 months per year during Period 3 (late melting, early freezing) and ~8 months per year during Period 4 (early melting, early freezing) (Extended Data Fig. 2).

Our results are supported by East Antarctic ice core records, which demonstrate that heavy spring sea-ice conditions generally occurred during periods of cool air temperatures over the East Antarctic Plateau and Wilkes Land coast[19]. However, Period 4 experienced low air temperatures and early autumn sea-ice return, but early sea-ice retreat (Section 2 in the Supplementary Information). This, along with discrepancies at the decadal scale, may explain the non-significant anti-correlations between the marine and ice core records (Section 4 in the Supplementary Information). However, the good centennial to multi-centennial agreement indicates a close coupling between atmospheric and coastal oceanic conditions at these timescales.

We then compared natural sea-ice variability off ALC with Indian APF oceanographic conditions. Diatom assemblages in COR1GC core indicate that sea ice never reached the core location from 0 to 1000 CE. We thus used SST as an alternative indicator, whereby higher SSTs infer a more southern winter sea-ice edge[20]. Diatoms are robust and commonly used tools to quantitatively reconstruct SST in the open SO[21] (Methods). The COR1GC record (Fig. 2d) shows mean SST of ~4.5 °C during Period 1 and early Period 3, and SST of ~3 °C during Period 2. Over the common period, the *F. curta* group (Hole U1357B, ALC) and SST (COR1GC, Indian APF) records are significantly and positively correlated (Section 4 in the Supplementary Information), demonstrating that cold waters and heavy SIP in ALC were congruent with warm surface ocean conditions at the Indian APF (Periods 1 and 3). Conversely, lower SIP and warmer conditions in ALC were synchronous with colder surface ocean conditions at the Indian APF (Period 2). Therefore, an important finding of our study is that there was opposite climate variability between the high and mid-latitudes of the Indian SO over the last 2,000 years. A similar behaviour has been previously observed at millennial timescales over the Holocene and attributed to changes in the latitudinal insolation and thermal gradients[9] through their impact on the southern westerly winds (SWW), the eastward zonal atmospheric circulation between 30° and 60° S that influences large-scale precipitation patterns and ocean circulation in the SO.

Drivers inferred from data and DA

Deciphering between changes in intensity and position of the SWW over the last 2,000 years is complex. However, two SWW records, based on different proxies (iron content and foraminifer geochemistry) and processes (precipitation and hydrologic front migration), give a robust picture of latitudinal shifts in the SWW[22,23]. The two wind records are significantly correlated, while the Fe content record in core GeoB3313-1 is significantly correlated with the SST record, and the *Globorotalia inflata* $\delta^{18}O$ record in core GeoB13862-1 is significantly correlated with the *F. curta* group record (Section 4 in the Supplementary Information). Taken together, the two wind records suggest that the core of the SWW was generally located southward during Periods 1 and 3 and located northward during Periods 2 and 4 (Fig. 2e,f). The sodium content in Antarctic ice cores provides further insight into the atmospheric circulation during these periods. Sodium content is a direct and conservative tracer of marine source air-mass intrusion, with higher content indicating greater poleward transport of warm, moist air at the southernmost limb of the SWW[24]. Ice cores from Wilkes Land (Law Dome), the East Antarctic Plateau (Dome C) and West Antarctica (Taylor Dome and Siple Dome) generally show greater Na content during

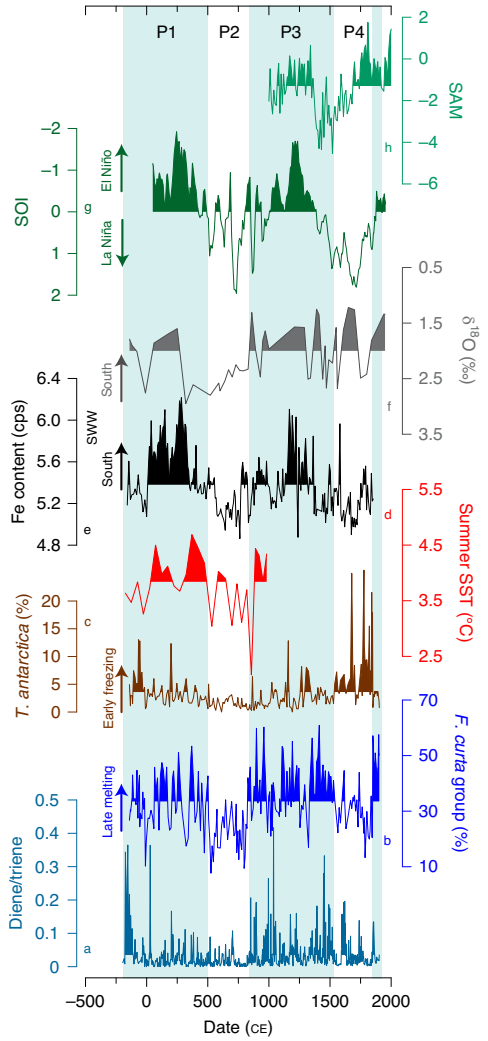

Fig. 2 | Intercomparison of sea-ice and climate records over the last 2,000 years. a, Diene/triene ratio in IODP Hole U1357B (this study). **b**, Relative abundances of the *F. curta* group in Hole U1357B (this study). **c**, Relative abundances of *Thalassiosira antarctica* in Hole U1357B core (this study). **d**, Mean summer SSTs estimated from diatom-based transfer function in COR1GC core (this study). **e**, Iron content in GeoB3313-1 core with higher values indicating a poleward position of the southern westerly winds (SWW)[22]. **f**, Ice-volume-corrected *Globorotalia inflata* $\delta^{18}O$ record in GeoB13862-1 core, with lower values indicating meridional shifts of the Brazil–Malvinas Confluence and SWW[23]. **g**, Southern Oscillation Index (SOI) record calculated as the difference between the reconstructed precipitation records from Indonesia and the Galapagos[49]. **h**, Southern Annular Mode (SAM) record calculated from an array of temperature-sensitive proxy records in Antarctica and South America[50].

Periods 1 and 3, relative to Period 2, supporting a poleward position and more intense SWW when SSTs at the Indian APF were higher and sea ice in the ALC region was more persistent (Section 3 in the Supplementary Information). However, the relationship lessens over Period 4 with, generally, high Na content in ice cores but less-persistent sea ice in ALC.

DA is a mathematical method that optimally combines information from proxy records and climate physics as represented by a climate model. It has been applied here to understand how large-scale atmospheric reorganization could drive decadal-to-centennial variability of Antarctic sea ice over the last 2,000 years and to identify processes that led to the opposite climate trends between the high and mid-latitudes of the Indian SO. The simulations selected are an ensemble of experiments covering the past millennium performed with the CESM1-CAM5 coupled climate model[25]. This model has a good performance at high southern latitudes and has been widely used for Antarctic studies[26]. We have assimilated both COR1GC SST and Hole U1357B sea-ice records (Methods), along with seven Antarctic ice core-based regional surface temperature reconstructions, to ensure the coherency with continental conditions[27]. From a technical point of view, DA was able to reconstruct variations of assimilated variables (the average of the linear correlations between the assimilated variables and those reconstructed is 0.86; section 5.1 in the Supplementary Information). This means that no inconsistency is found between atmospheric and oceanic temperature reconstructions, and particularly between the opposite climate patterns in ALC and Indian APF regions. Two composites were built to understand the mechanisms underlying the variations at each oceanic core site (Methods). First, the SST+/SIC+ (SIC, sea-ice concentration) composite represents climate conditions when COR1GC SST and Hole U1357B SIP anomalies were concomitantly positive or concomitantly negative. Second, the SST+/SIC– composite represents climate conditions when positive anomalies of SST at COR1GC were congruent to negative anomalies of SIP at Hole U1357B, and vice versa.

The SST+/SIC+ composite corresponds to 65% (about two-thirds) of the 0–1000 CE interval, when our records overlap, confirming the general anti-correlation between our palaeorecords over this period. The model reproduces the anti-correlation between the two regions as inferred from the data, for surface air temperatures (SATs), SSTs and SIC (Fig. 3, left). Low modelled SATs and SSTs are reconstructed in the southwestern Pacific and the ALC region, while high SATs and SSTs are obtained in the Bellinghausen–Amundsen Sea and in the Indian APF. Sea-ice modelled distribution is opposite to both SAT and SST with greater SIC in the ALC region but lower concentration in the Bellinghausen–Amundsen Sea and in the Indian APF, indicating a reduced extent there. In the DA-based reconstruction, these climate conditions are associated with a strong negative anomaly of geopotential height in the southern mid-latitudes of the Pacific and eastern Indian sectors and a strong positive anomaly of geopotential height over the Bellinghausen–Amundsen Sea. Such an atmospheric pattern resembles a negative phase of the Southern Oscillation Index (SOI; a key atmospheric index for gauging the strength of El Niño and La Niña events) as encountered today during El Niño-like conditions[28,29]. In the DA-based reconstruction, a mean SOI value of −0.34 ($P<0.05$; section 5.2 in the Supplementary Information) confirms that El Niño-like conditions prevailed for the SST+/SIC+ composite. This is further supported by the simulation of pervasive warm temperature anomalies in the Equatorial Pacific (section 5.3 in the Supplementary Information). However, the pattern is not strictly Pacific centred, and a non-significant annular component is evidenced along with a negative phase of the Southern Annular Mode (SAM, the dominant mode of extra-tropical atmospheric variability in the Southern Hemisphere related to changes in the mid- to high-latitudinal meridional pressure gradient and in variations in the strength and position of the SWW; index of −0.67, $P<0.05$). This indicates a combined effect of El Niño Southern Oscillation (ENSO) and SAM to modulate SST and sea-ice fields in the Indian SO at the decadal-to-centennial timescales. In the DA-based reconstruction, the combination of El Niño and SAM– resulted in the climate situation described in the preceding while the combination of La Niña and SAM+ led to the opposite climate situation, with lower SST in the Indian APF and shorter sea-ice duration in the ALC region but overall larger sea-ice extent in the Indian sector.

These DA-based results are supported by palaeoclimate data whereby significant correlations are found between our SST and sea-ice records, SWW records and the SOI (Section 4 in the

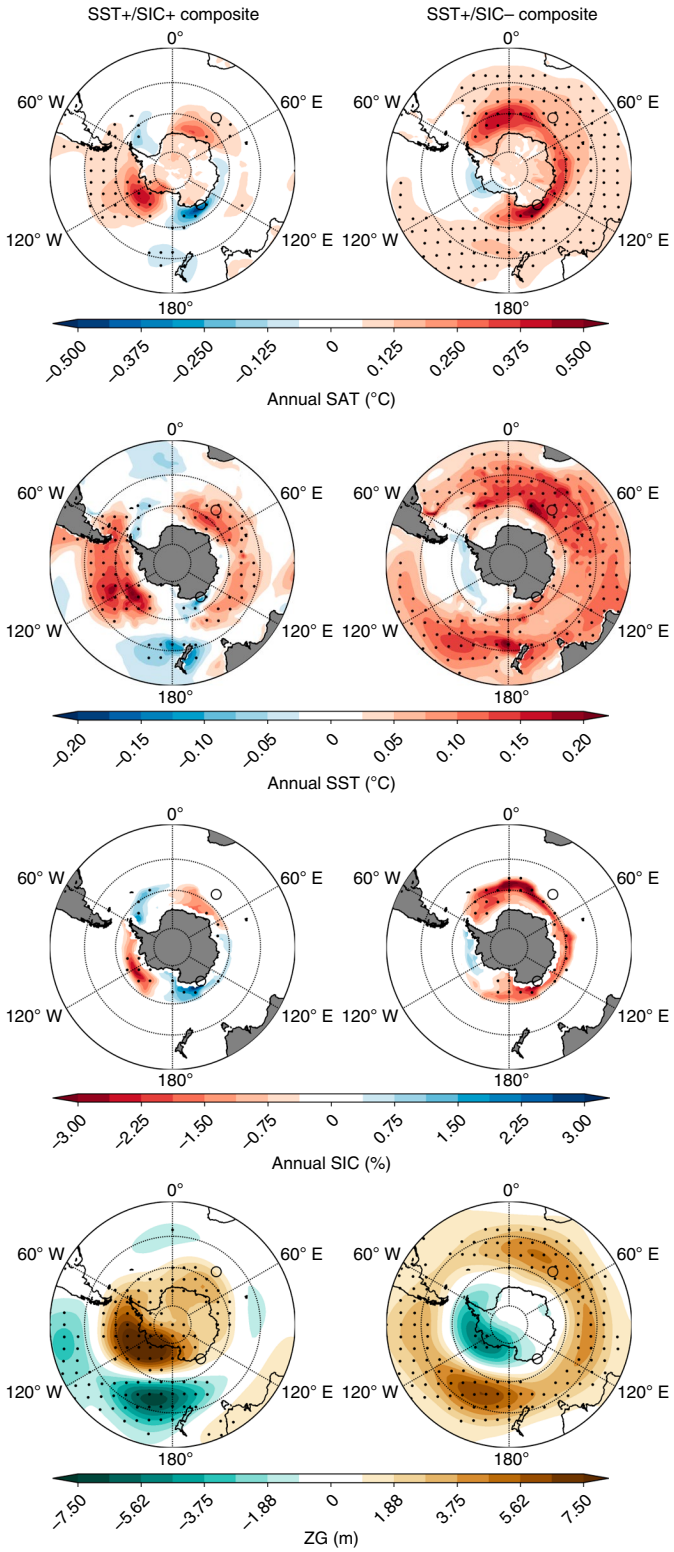

Fig. 3 | Mean environmental conditions for the SST+/SIC+ composite and the SST+/SIC– composite based on offline DA using the CESM1-CAM5 model outputs. Values represent anomalies to the first millennium (0–1000 CE) as reference. Circles represent the geographical locations of the two cores studied here (IODP Hole U1357B off Adélie Land and COR1GC around the Indian APF). ZG, geopotential height.

Supplementary Information). Multi-decadal negative phases of the SOI (El Niño-like conditions) are observed during periods 1 and 3, while positive phases of the SOI (La Niña-like conditions) are recorded during periods 2 and 4 (Fig. 2g). SOI and SAM appear negatively related during the 1000–1600 CE interval (Fig. 2g,h) but uncorrelated over the 1600–1800 CE interval when the sea-ice record in Hole U1357B is no longer in agreement with ice core records (sections 2 and 3 in the Supplementary Information). A recent study also identified a pervasive negative correlation between these two modes over the past millennium, despite a few intervals of weak or positive correlation[30]. During El Niño/SAM– (and La Niña/SAM+) combinations, atmospheric circulation in the mid-latitudes of the Pacific acts to maintain teleconnections with the equatorial Pacific[31], thus conveying low-latitude climate anomalies to the SO. In this configuration, recent El Niño events induced cool ocean temperatures and heavier sea-ice conditions off East Antarctica that were contrasted by warmer ocean temperatures at the Indian APF[32], as observed in our DA-based reconstruction. Mechanistically, our data, along with recent observations and modelling studies, suggest that warming of Indian APF waters (40–60° S) during El Niño events is related to the poleward intrusion of warm subtropical air masses[29,33] and surface waters when SWW are located further to the south[34], with a more southward direction[35]. Both processes induce sea-ice loss at the margin and equilibrate the sea-ice edge southward[36]. A positive feedback involving ocean–atmosphere heat exchange and absorption of solar energy may further warm the newly ice-free ocean region[37]. Cooling of high-latitude waters (south of 60° S) and heavier coastal sea-ice conditions are due mainly to reduced sea-ice transport northward[1] and sea-ice compaction by more northerly winds[38,39].

The SST+/SIC– composite corresponds to 35% (about one-third) of the 0–1000 CE interval. The DA-based results display high SATs and SSTs alongside a drop in SIC around Antarctica, thus suggesting a reduced sea-ice extent in the Indian sector. These conditions are associated with a negative anomaly of geopotential height over West Antarctica and an annular positive anomaly in the mid-latitudes (Fig. 3, right). Such a pattern in geopotential height resembles a positive phase of the SAM[40]. The SAM index value for the SST+/SIC– composite is 0.49 ($P < 0.05$; section 5.2 in the Supplementary Information), while the equatorial Pacific does not seem to play any significant role with an SOI index of 0.08 ($P > 0.05$; section 5.3 in the Supplementary Information). Observations and model studies suggest that the SO response to SAM+ like events depends on the timescale. The annual transient response is marked by enhanced Ekman upward pumping and northward transport of cold winter waters in the region of seasonal sea ice, cooling the surface and allowing sea-ice expansion[8,41]. However, at the multi-decadal timescale, sustained Ekman pumping results in increased upwelling of deep warm waters, warming the surface waters and reducing both SIC and sea-ice extent[6,36,41]. As such, the SST and sea-ice distributions observed in the SST+/SIC– composite are consistent with the longer-term response to prolonged positive SAM conditions.

Our new SST and sea-ice data along with our DA results indicate a strong regional heterogeneity in Indian SO natural climate variability over the last 2,000 years. According to our results, ENSO and SAM, as well as their phasing, are the key drivers of this climate heterogeneity. Of particular interest, the multi-decadal response to repetitive El Niño events or persistent SAM positive phase is a warming of the mid-latitudes that restricts the outer pack-ice extent in the Indian sector. Given the projected future increase in the frequency of extreme El Niño events[42] and of a prevalent positive SAM[43], our results suggest that these two climate modes will independently enhance sea-ice decline in the next decades and may oppose other potential stabilizing mechanisms such as increased fresh meltwater flux from glacial meltwater[44]. However, the global impact will depend on the phasing of these two climate modes. Our study adds to a growing body of evidence[7] that most state-of-the-art climate models do not adequately reconstruct SO natural variability,

and the new data provided here may be crucial to help better evaluate the reliability of these climate models.

Online content

Any methods, additional references, Nature Research reporting summaries, source data, extended data, supplementary information, acknowledgements, peer review information; details of author contributions and competing interests; and statements of data and code availability are available at https://doi.org/10.1038/s41561-021-00697-1.

Received: 11 March 2020; Accepted: 19 January 2021;
Published online: 22 February 2021

References

1. Hobbs, W. R. et al. A review of recent changes in Southern Ocean sea ice, their drivers and forcings. *Glob. Planet. Change* **143**, 228–250 (2016).
2. Rintoul, S. R. The global influence of localized dynamics in the Southern Ocean. *Nature* **558**, 209–218 (2018).
3. Parkinson, C. A 40-yr record reveals gradual Antarctic sea ice increases followed by decreases at rates far exceeding the rates in the Arctic. *Proc. Natl Acad. Sci. USA* **116**, 14414–14423 (2019).
4. Kwok, R., Comiso, J. C., Lee, T. & Holland, P. R. Linked trends in the South Pacific sea ice edge and Southern Oscillation Index. *Geophys. Res. Lett.* **43**, 10295–10302 (2016).
5. Meehl, G. A., Arblaster, J. A., Bitz, C. M., Chung, C. T. Y. & Teng, H. Antarctic sea-ice expansion between 2000 and 2014 driven by tropical Pacific decadal climate variability. *Nat. Geosci.* **9**, 590–595 (2016).
6. Ferreira, D., Marshall, J., Bitz, C. M., Solomon, S. & Plumb, A. Antarctic Ocean and sea ice response to ozone depletion: a two-time-scale problem. *J. Clim.* **28**, 1206–1226 (2015).
7. Jones, J. M. et al. Assessing recent trends in high-latitude Southern Hemisphere surface climate. *Nat. Clim. Change* **6**, 917–926 (2016).
8. Purich, A., Cai, W., England, M. H. & Cowan, T. Evidence for link between modelled trends in Antarctic sea ice and underestimated westerly wind changes. *Nat. Commun.* **7**, 10409 (2016).
9. Denis, D. et al. Sea ice and wind variability during the Holocene in East Antarctica: insight on middle–high latitude coupling. *Quat. Sci. Rev.* **29**, 3709–3719 (2010).
10. Divine, D. et al. Holocene Antarctic climate variability from ice and marine sediment cores: insights on ocean–atmosphere interaction. *Quat. Sci. Rev.* **29**, 303–312 (2010).
11. Peck, V. L., Allen, C. S., Kender, S., McClymont, E. R. & Hodgson, D. A. Oceanographic variability on the West Antarctic Peninsula during the Holocene and the influence of upper circumpolar deep water. *Quat. Sci. Rev.* **119**, 54–65 (2015).
12. Mezgec, K. et al. Holocene sea ice variability driven by wind and polynya efficiency in the Ross Sea. *Nat. Commun.* **8**, 1334 (2017).
13. Ashley, K. E. et al. Mid-Holocene Antarctic sea-ice increase driven by marine ice sheet retreat. *Clim. Past* **17**, https://doi.org/10.5194/cp-17-1-2021 (2021).
14. Orme, L. et al. Sea-surface temperature in the Indian sector of the Southern Ocean over the Late Glacial and Holocene. *Clim. Past* **16**, 1451–1467 (2020).
15. Campagne, P. et al. Sedimentary response to sea ice and atmospheric variability over the instrumental period off Adélie Land, East Antarctica. *Biogeosciences* **13**, 4205–4218 (2016).
16. Smik, L., Belt, S. T., Lieser, J. L., Armand, L. K. & Leventer, A. Distributions of highly branched isoprenoid alkenes and other algal lipids in surface waters from East Antarctica: further insights for biomarker-based paleo sea-ice reconstruction. *Org. Geochem.* **95**, 71–80 (2016).
17. Pike, J. et al. Observations on the relationship between the Antarctic coastal diatoms *Thalassiosira antarctica* Comber and *Porosira glacialis* (Grunow) Jørgensen and sea ice concentrations during the Late Quaternary. *Mar. Micropaleontol.* **73**, 14–25 (2009).
18. Armand, L. K., Crosta, X., Romero, O. & Pichon, J.-J. The biogeography of major diatom taxa in Southern Ocean sediments: 1. Sea ice related species. *Palaeogeogr. Palaeoclimatol. Palaeoecol.* **223**, 93–126 (2005).
19. Stenni, B. et al. Antarctic climate variability on regional and continental scales over the last 2000 years. *Clim. Past* **13**, 1609–1634 (2017).
20. Gordon, A. L. Seasonality of Southern Ocean sea-ice. *J. Geophys. Res.* **86**, 4193–4197 (1981).
21. Esper, O. & Gersonde, R. Quaternary surface water temperature estimations: new diatom transfer functions for the Southern Ocean. *Palaeogeogr. Palaeoclimatol. Palaeoecol.* **414**, 1–19 (2014).
22. Varma, V., Prange, M., Lamy, F., Merkel, U. & Schulz, M. Solar-forced shifts of the Southern Hemisphere Westerlies during the Holocene. *Clim. Past* **7**, 339–347 (2011).
23. Voigt, I., Chiessi, C. M., Piola, A. R. & Henrich, R. Holocene changes in Antarctic Intermediate Water flow strength in the Southwest. *Palaeogeogr. Palaeoclimatol. Palaeoecol.* **463**, 60–67 (2016).
24. Mayewski, P. et al. Ice core and climate reanalysis analogs to predict Antarctic and Southern Hemisphere climate changes. *Quat. Sci. Rev.* **155**, 50–66 (2017).
25. Otto-Bliesner, B. L. et al. Climate variability and change since 850 CE: an ensemble approach with the Community Earth System Model. *Bull. Am. Meteor. Soc.* **97**, 735–754 (2016).
26. Landrum, L. L., Holland, M. M., Raphael, M. N. & Polvani, L. M. Stratospheric ozone depletion: an unlikely driver of regional trends in Antarctic sea ice in austral fall in the late twentieth century. *Geophys. Res. Lett.* **44**, 11062–11070 (2017).
27. Klein, F. et al. Assessing the robustness of Antarctic temperature reconstructions over the past two millennia using pseudoproxy and data assimilation experiments. *Clim. Past* **15**, 661–684 (2019).
28. Turner, J. The El Niño–Southern Oscillation and Antarctica. *Int. J. Climatol.* **24**, 1–31 (2004).
29. Yuan, X. ENSO-related impacts on Antarctic sea ice: a synthesis of phenomenon and mechanisms. *Antarct. Sci.* **16**, 415–425 (2004).
30. Dätwyler, C. et al. Teleconnections and relationship between the El Niño–Southern Oscillation (ENSO) and the Southern Annular Mode (SAM) in reconstructions and models over the past millennium. *Clim. Past* **16**, 743–756 (2020).
31. Fogt, R. L., Bromwich, D. H. & Hines, K. M. Understanding the SAM influence on the South Pacific ENSO teleconnection. *Clim. Dyn.* **36**, 1555–1576 (2011).
32. Ciasto, L. M., Simpkins, G. R. & England, M. H. Teleconnections between tropical Pacific SST anomalies and extratropical Southern Hemisphere climate. *J. Clim.* **28**, 56–65 (2015).
33. Nicolas, J. P. et al. January 2016 extensive summer melt in West Antarctica favoured by strong El Niño. *Nat. Commun.* **8**, 15799 (2017).
34. Delworth, T. L. & Zeng, F. Simulated impact of altered Southern Hemisphere winds on the Atlantic Meridional Overturning Circulation. *Geophys. Res. Lett.* **35**, L20708 (2008).
35. Meehl, G. A. et al. Sustained ocean changes contributed to sudden Antarctic sea ice retreat in late 2016. *Nat. Commun.* **10**, 14 (2019).
36. Fan, T., Deser, C. & Schneider, D. P. Recent Antarctic sea ice trends in the context of Southern Ocean surface climate variations since 1950. *Geophys. Res. Lett.* **41**, 2419–2426 (2014).
37. Masson-Delmotte, V. et al. Past and future polar amplification of climate change: climate model intercomparisons and ice-core constraints. *Clim. Dyn.* **26**, 513–529 (2006).
38. Turner, J., Harangozo, S. A., Marshall, G. J., King, J. C. & Colwell, S. R. Anomalous atmospheric circulation over the Weddell Sea, Antarctica, during the austral summer of 2001–02 resulting in extreme sea ice conditions. *Geophys. Res. Lett.* **29**, 2160 (2002).
39. Sugimoto, F. et al. Interannual variability in sea-ice thickness in the pack-ice zone off Lützow-Holm Bay, East Antarctica. *Polar Sci.* **10**, 43–51 (2016).
40. Thompson, D. W. J. & Solomon, S. Interpretation of recent Southern Hemisphere climate change. *Science* **296**, 895–899 (2002).
41. Kostov, Y. et al. Fast and slow responses of Southern Ocean sea surface temperature to SAM in coupled climate models. *Clim. Dyn.* **48**, 1595–1609 (2017).
42. Cai, W. et al. Increasing frequency of extreme El Niño events due to greenhouse warming. *Nat. Clim. Change* **4**, 111–116 (2014).
43. Arblaster, J. A. & Meehl, G. A. Contributions of external forcings to Southern Annular Mode trends. *J. Clim.* **19**, 2896–2905 (2006).
44. Bintanja, R., van Oldenborgh, G. J., Drijfhout, S. S., Wouters, B. & Katsman, C. A. Important role for ocean warming and increased ice-shelf melt in Antarctic sea-ice expansion. *Nat. Geosci.* **6**, 376–379 (2013).
45. Locarnini, R. A. et al. *World Ocean Atlas 2009, Volume 1: Temperature* NOAA Atlas NESDIS 68 (ed. Levitus, S.) (US Government Printing Office, 2010).
46. Orsi, A. H., Whitworth, T. & Nowlin, W. D. On the meridional extent and fronts of the Antarctic Circumpolar Current. *Deep Sea Res.* **42**, 641–673 (1995).
47. Schweitzer, P. N. *Monthly Averaged Polar Sea-Ice Concentration* (USGS, 1995).
48. International Hydrographic Organization *Limits of Oceans and Seas* 3rd edn (Imp. Monégasque, 1953).
49. Yan, H. et al. A record of the Southern Oscillation index for the past 2,000 years from precipitation proxies. *Nat. Geosci.* **4**, 611–614 (2011).
50. Abram, N. J. et al. Evolution of the Southern Annular Mode during the past millennium. *Nat. Clim. Change* **4**, 564–569 (2014).

Methods

Location and description of the cores. IODP Expedition 318 was conducted in January–February 2010 and drilled three holes at U1357 Site (66° 25' S, 140° 26' E, 1,026 m water depth, located ~35 km from the coast of Adélie Land), in the most proximal depression of the Dumont d'Urville Trought (DDUT), through the Holocene sediment sequence. Hole U1357B recovered an ~172-m-long archive, in 19 sections, of undisturbed hemipelagic sediments composed of unusually pure diatom oozes[51]. The upper 170 m of the core is characterized by dark olive-brown to light greenish-brown diatom oozes, along with centimetre-scale laminations, as previously shown at the same site[51]. Laminations result from changing conditions between a high-productivity deposition during spring and a less organic-rich sedimentation during summer[52–54].

The 2.5-m-long COR1GC core was retrieved from the southwest flank of the Conrad Rise in the southwestern Indian sector of the SO (54° 16' S, 39° 46' E, 2834 m water depth) using a gravity corer during the expedition KH-10-7 on board the R/V *Hakuho-Maru* in 2010. COR1GC sediments are composed mainly of homogeneous pale-yellow to greenish diatom oozes[55].

Chronologies of the cores. The age model of Hole U1357B core is based on 87 radiocarbon dates performed on acid-insoluble bulk organic carbon[13]. The raw dates were calibrated with a reservoir age correction of 1,200 ± 100 years recommended for the area[56]. An additional correction of 400 years to account for the dead carbon fraction was applied. The dead carbon fraction has been calculated via the comparison of radiocarbon dates on bulk organic carbon and foraminifera in the twin JPC17 core[57]. The depth–age conversion was done using BACON[58] and the Marine13 calibration dataset[59]. The core covers the last 11,500 years in 172 m and the last 2,000 years in 40 m with a mean sedimentation rate of 2 cm yr^{-1}. The last 2,000 years are constrained by 24 dates. More details can be found in ref. [13].

The age model of COR1GC is based on 15 radiocarbon dates performed on monospecific samples of the planktic foraminifera *Neogloboquadrina pachyderma* sinistral[14]. The raw dates were calibrated with a reservoir age correction of 890 ± 100 years recommended for the area[60]. The depth–age conversion was done using BACON[58] with the Marine13 calibration dataset[59]. The core covers the 1,000–14,000 yr period in 2.5 m and the 1,000–2,000 yr period in 0.5 m with a mean sedimentation rate of 0.025 cm yr^{-1}. The last 2,000 years are constrained by five dates. More details can be found in ref. [14].

Diatom analysis. Diatom permanent slides were made according to the technique described in ref. [61]. Briefly, the sediment is dried overnight in an oven at 60 °C. Around 0.5 g of dry sediment is transferred into a 250 ml beaker and covered with H_2O_2 at 30%. The beaker is left in a hot bath at 65 °C until the reaction stops. It might be necessary to add H_2O_2 a second time as this chemical loses its oxidative power during the reaction. The solution is then transferred into a tube and washed three times by adding 50 ml distilled water and centrifuged for 7 min at 1,250 rpm. Then, carbonates are dissolved by adding 10–20 ml HCl at 30% and the solution is washed again three times. The sediment is subsequently transferred back into the beaker and dilution is adjusted to 50–100 ml by adding distilled water. A few drops (150 µl each) are deposited into a petri dish in which a coverslip was placed and covered with distilled water. The petri dish is then filled with distilled water. After half an hour, the water is slowly removed from the petri dish by adding a cotton string. Dried coverslips on which the sediment is now deposited are glued permanently on a microscope slide using NOA61. Three slides are mounted per sample.

Around 350 complete diatom valves were counted per sample with a phase contrast Olympus BX-51 microscope at a magnification of ×1,000. Diatoms were identified to species or species group level, and the relative abundance of each was determined as the fraction of diatom species against total diatom abundance in the sample.

In core COR1GC, diatoms were counted every ~1 cm, providing a temporal resolution of 30–60 years (mean resolution of ~50 years) over the considered period.

In Hole U1357B, diatoms were counted every 5–20 cm, providing a temporal resolution of 3–15 years (mean resolution of ~10 years) over the considered period.

Biomarker analysis. HBI alkenes (diene and trienes) were extracted from the sediment following the method described in ref. [62]. To ~0.5 g of freeze-dried sediment, 9 ml CH_2Cl_2/MeOH (2/1, v/v), containing an internal standard (7-hexylnonadecane (7-HND)), was added. Sonication and centrifugation steps were repeated thrice to extract properly the selected compounds. After drying with N_2 at 35 °C, the total lipid extract was fractionated over a silica column into apolar and polar fractions using 3 ml hexane and 6 ml CH2Cl2/MeOH (1/1, v/v), respectively. HBIs were obtained from the apolar fraction by the fractionation over a silica column using hexane as eluent following the procedures reported by refs. [62,63]. After removing the solvent with N_2 at 35 °C, elemental sulfur was removed using the tetrabutylammonium sulfite method[64,65]. The hydrocarbon fraction was analysed by an Agilent 7890 A gas chromatograph (GC) fitted with 30 m fused silica Agilent J&C GC columns (0.25 mm ID and 0.25 µm film thickness) and coupled to an Agilent 5975 C Series mass selective detector with triple axis detector. Spectra were collected using the Hewlett-Packard MS-Chemstation software. Relative abundances of individual HBI isomers were calculated on the basis of their individual GC retention times and mass spectra (m/z 346; m/z 348) relative to those of the internal standard (m/z 266). Values are expressed as concentration relative to the 7-HND.

In Hole U1357B, HBIs were analysed every 5 cm, providing a temporal resolution of ~3 years.

Modern sea-ice data. Daily SICs for the period 1979–2012 were obtained from the National Snow and Ice Data Center data repository. The dataset is based on passive microwave observations from the Nimbus-7 SSMR (1979–1987) and DMSP SSM/I (1987–2007) and SSMIS (2007–2012) radiometers processed with the NASA Team algorithm[66] at a spatial resolution of 25 × 25 km. Averaged SICs were calculated over the core site in the central part of the DDUT. Two pixels centred at 66.5481° S, 140.5149° E and 66.4065° S, 140.0883° E were used for the extraction of the daily SIC values[15].

The sea-ice retreat date was determined as the Julian day when the SIC (7-day average) dropped below 40%, while the sea-ice advance was attributed to the day when SIC increased to above 40%. The duration of the ice-free season corresponds to the number of days per year during which SIC < 40%. Monthly anomalies are expressed relative to the mean value calculated for each month over the 1979–2009 period[15].

Reconstruction of summer SSTs in core COR1GC (Indian APF). Diatoms are widely used to reconstruct past variations in SSTs and SIP in the SO at different timescales. Several transfer functions have been developed to quantify past SST[21,67] and SIP[68,69].

A summer (January–February–March) SST reconstruction in core COR1GC was achieved by applying the modern analogue technique (MAT) to fossil diatom assemblages. The modern database is composed of 249 surface sediment samples (modern analogues) for which locations modern summer SSTs were interpolated on a 1° × 1° grid from the World Ocean Atlas 2013[45] using Ocean Data View[70]. The MAT is based on the principle that similar species assemblages are derived from similar environments[71]. The MAT used here was implemented from the 'bioindic' package[72] built on the R-platform (http://cran.r-project.org/). We used here the relative abundances of 32 diatom species and the chord distance to select the five most similar modern analogues. The threshold above which modern analogues are supposed to be too dissimilar to the fossil assemblage is fixed at the first quartile of random distances on the validation/modern dataset. Quantitative estimates of summer SST represent a distance-weighted mean of the climate values associated with the selected modern analogues[73]. For summer SST, this method yields an R^2 of 0.96 and a root mean square error of prediction of ~1 °C.

Reconstruction of sea-ice conditions in site IODP U1375B (ALC). Diatom transfer functions do not perform well on the coastal Antarctic shelves, preventing a robust quantification of past sea-ice changes. Fortunately, diatom relative abundances are still an extremely useful tool to qualitatively reconstruct both SST and sea-ice conditions in regions where transfer functions do not perform well. However, palaeoclimate models assimilate only quantitative data such as SST and SIP. We have developed a protocol to convert diatom relative abundances to quantitative SIP data.

Off Adélie Land, ref. [15] has shown that relative abundances of the open-water diatom (OWD) group over the past 40 years were strongly related to the length of the open-water season. At the inter-annual to decadal timescale, this relationship appears stronger than the one linking the *F. curta* group to sea-ice conditions, probably because of highly variable conditions during spring and more stable conditions during summer. The relative abundances of the OWD group were resampled at an annual resolution over the 40 years covered by core DTCI2010, retrieved at the same location as site IODP U1375B, for a direct comparison with the mean annual open-water length. The mean annual length of the open-water, ice-free season is understood as the period when SIC consistently falls below 40% in spring and increases back above 40% in autumn (section Modern sea-ice data in the Methods). Resampling did not change the inter-annual pattern of the OWD group but reduced the amplitude of the variability (Extended Data Fig. 1a).

The resampled OWD group record was then compared with the yearly sea-ice-free season. Both records show similar decadal variability (Extended Data Fig. 1b). Two endmembers were defined. The upper one represents high OWD group relative abundances and a long ice-free season while the lower one represents low OWD group relative abundances and a short ice-free season (Extended Data Fig. 1b, grey shaded boxes). These endmembers were used to calculate a linear relationship linking OWD group relative abundances and the length of the open-water season (Extended Data Fig. 1c).

Finally, the relative abundances of the OWD group in Hole U1357B were injected into the equation derived from the modern time to quantify the mean annual length of the open-water season over the last 2,000 years at a 5–20 yr resolution (Extended Data Fig. 2, orange line). The mean annual length of the sea-ice duration was then quantified by subtracting the open-water values from 365 days (Extended Data Fig. 2, blue line).

DA method. DA, optimally combining information from proxy records and model simulations, is now a standard procedure in palaeoclimatology[74,75]. In this study, we use an offline method. This means that the model prior is obtained from an ensemble of existing model simulations and that this ensemble does not evolve as a function of the results of any previous assimilation[74]. Consequently, in contrast to online DA methods, information is not propagated forward in time. However, this method is affordable and can be applied in palaeoclimatology on high-resolution climate models—something almost impossible with online methods as DA requires a large ensemble of simulations. As a result, the offline DA has provided skilful reconstructions for various kinds of data spanning recent centuries[25,76–78]. The method used here is based on a particle filter[79] following the implementation described in ref. [80]. Throughout the DA procedure, we computed the likelihood of each ensemble member (also called particle) by comparing its results with the assimilated proxy-based reconstruction. A weight was attributed to each particle as a function of its likelihood. The weighted mean of all particles provided the DA-based reconstruction for each time step. To construct our reanalysis product, we used the multi-members CESM1-CAM5 outputs (12 simulations, ref. [25]) covering the 850–2005 CE period.

DA experimental design. We assimilated the regional Antarctic continental reconstructions of surface temperature from ref. [27], the summer SST at COR1GC as well as the length of the ice-free season (ocean without sea ice) at Hole U1357B. Including data derived from ice cores provided a stronger constraint for the assimilation procedure and ensured that the reconstructed patterns not only were valid for the ocean data but also are consistent with the temperature changes observed on the continent. The time frequency for DA is 10 years, comparable to Hole U1357B resolution. The COR1GC core, which has a multi-decadal resolution, was linearly interpolated on the decadal scale. Conversely, the annual surface temperature reconstructions of ref. [27] have been averaged over 10 years.

Two composites were built from the two oceanic core records to understand the mechanisms underlying the variations at each oceanic core site (COR1GC and Hole U1357B; Fig. 3).

First, the SST+/SIC+ composite was obtained by computing the average of all the 10 yr periods when COR1GC and Hole U1357B series were in phase, indicating opposite climate conditions in the two studied areas (positive anomalies of SST at COR1GC and positive anomalies of the sea-ice duration at Hole U1357B, and vice versa). To obtain a common signal from opposite conditions, we added the mirror image of the SST-/SIC- composite to the SST+/SIC+ composite.

Second, the SST+/SIC- composite was obtained by computing the average of all the 10 yr periods when COR1GC and Hole U1357B series were opposite, indicating similar climate conditions in the two studied areas (positive anomalies of SST at COR1GC and negative anomalies of the sea-ice duration at Hole U1357B, and vice versa). To obtain a common signal from opposite conditions, we added the mirror image of the SST–/SIC+ composite to the SST+/SIC– composite.

Anomalies are computed using the first millennium (0–1000 CE) as reference.

Atmospheric indices in the climate model. The SAM index is calculated as the normalized difference in zonal 500 hPa geopotential height between the latitudes 40° S and 65° S, while the SOI index is the normalized difference in 500 hPa geopotential height between Tahiti and Darwin.

Data availability

Diatom-based sea surface temperature data from core COR1GC can be found at https://doi.org/10.1594/PANGAEA.913621. Diatom and highly branched isoprenoid data from IODP Hole U1357B are available at https://doi.org/10.1594/PANGAEA.924721 and https://doi.org/10.1594/PANGAEA.924723, respectively.

Code availability

The results of the Last Millennium Ensemble performed with the CESM1 model are available at https://www.earthsystemgrid.org/dataset/ucar.cgd.ccsm4.CESM_CAM5_LME.html.

References

51. Escutia, C., Brinkhuis, H., Klaus, A. & Expedition 318 Scientists *Expedition 318 Summary* https://doi.org/10.2204/iodp.proc.318.101.2011 (2011).
52. Stickley, C. E. et al. Deglacial ocean and climate seasonality in laminated diatom sediments, Mac.Robertson Shelf, Antarctica. *Palaeogeogr. Palaeoclimatol. Palaeoecol.* **227**, 290–310 (2005).
53. Denis, D. et al. Seasonal and sub-seasonal climate changes recorded in laminated diatom ooze sediments, Adélie Land, East Antarctica. *Holocene* **16**, 1137–1147 (2006).
54. Maddison, E. J. et al. Post-glacial seasonal diatom record of the Mertz Glacier Polynya, East Antarctica. *Mar. Micropaleontol.* **60**, 66–88 (2006).
55. Ikehara, M. et al. Cruise report of the Hakuho-maru Cruise KH-10-7 (2010).
56. Ingólfsson, O. et al. Antarctic glacial history since the Last Glacial Maximum: an overview of the record on land. *Antarct. Sci.* **10**, 326–344 (1998).
57. Costa, E. et al. *Solar Forcing and El Niño–Southern Oscillation (ENSO) Influences on Productivity Cycles Interpreted from a Late-Holocene High-Resolution Marine Sediment Record, Adélie Drift, East Antarctic Margin* Short Research Paper 306 (USGS and The National Academies, 2007).
58. Blaauw, M. & Christeny, J. A. Flexible paleoclimate age-depth models using an autoregressive gamma process. *Bayesian Anal.* **6**, 457–474 (2011).
59. Reimer, P. J. et al. IntCal13 and Marine13 radiocarbon age calibration curves 0–50,000 years cal BP. *Radiocarbon* **55**, 1869–1887 (2013).
60. Butzin, M., Prange, M. & Lohmann, G. Radiocarbon simulations for the glacial ocean: the effects of wind stress, Southern Ocean sea ice and Heinrich events. *Earth Planet. Sci. Lett.* **235**, 45–61 (2005).
61. Crosta, X. et al. Last Abundant Appearance Datum of *Hemidiscus karstenii* driven by climate change. *Mar. Micropaleontol.* **157**, 101861 (2020).
62. Belt, S. T., Massé, G., Rowland, S. J. & Rohmer, M. Highly branched isoprenoid alcohols and epoxides in the diatom *Haslea ostrearia* Simonsen. *Org. Geochem.* **38**, 16–27 (2007).
63. Massé, G. et al. Highly branched isoprenoids as proxies for variable sea ice conditions in the Southern Ocean. *Antarct. Sci.* **23**, 487–498 (2011).
64. Jensen, S., Renberg, L. & Reutergardh, L. Residue analysis of sediment and sewage sludge for organochlorines in the presence of elemental sulphur. *Anal. Chem.* **49**, 316–318 (1977).
65. Riis, V. & Babel, W. Removal of sulfur interfering in the analysis of organochlorines by GC-ED. *Analyst* **124**, 1771–1773 (1999).
66. Cavalieri, D. J., Germain, K. M. S. & Swift, C. T. Reduction of weather effects in the calculation of sea ice concentration with the DMSP SSM/I. *J. Glaciol.* **41**, 455–464 (1995).
67. Crosta, X., Sturm, A., Armand, L. & Pichon, J.-J. Late Quaternary sea ice history in the Indian sector of the Southern Ocean as recorded by diatom assemblages. *Mar. Micropaleontol.* **50**, 209–223 (2004).
68. Esper, O. & Gersonde, R. New tools for the reconstruction of Pleistocene Antarctic sea ice. *Palaeogeogr. Palaeoclimatol. Palaeoecol.* **399**, 260–283 (2014).
69. Ferry, A. J. et al. First records of winter sea-ice concentration in the southwest Pacific sector of the Southern Ocean. *Paleoceanography* **30**, 1525–1539 (2015).
70. Schlitzer, R. Interactive analysis and visualization of geoscience data with Ocean Data View. *Comput. Geosci.* **28**, 1211–1218 (2012).
71. Prell, W. L. *The Stability of Low-Latitude Sea-Surface Temperatures: An Evaluation of the CLIMAP Reconstruction with Emphasis on the Positive SST Anomalies* Report TR 025 (US Department of Energy, 1985).
72. Guiot, J. & de Vernal, A. Is spatial autocorrelation introducing biases in the apparent accuracy of paleoclimatic reconstructions? *Quat. Sci. Rev.* **30**, 1965–1972 (2011).
73. Guiot, J. et al. The climate in western Europe during the last Glacial/Interglacial cycle derived from pollen and insect remains. *Palaeogeogr. Palaeoclimatol. Palaeoecol.* **103**, 73–93 (1993).
74. Goosse, H. et al. Antarctic temperature changes during the last millennium: evaluation of simulations and reconstructions. *Quat. Sci. Rev.* **55**, 75–90 (2012).
75. Steiger, N. J., Smerdon, J. E., Cook, E. R. & Cook, B. I. A reconstruction of global hydroclimate and dynamical variables over the Common Era. *Sci. Data* **5**, 1–15 (2018).
76. Matsikaris, A., Widmann, M. & Jungclaus, J. On-line and off-line data assimilation in palaeoclimatology: a case study. *Clim. Past* **11**, 81–93 (2015).
77. Hakim, G. J. et al. The last millennium climate reanalysis project: framework and first results. *J. Geophys. Res.* **121**, 6745–6764 (2016).
78. Steiger, N. J., Steig, E. J., Dee, S. G., Roe, G. H. & Hakim, G. J. Climate reconstruction using data assimilation of water isotope ratios from ice cores. *J. Geophys. Res. Atmos.* **122**, 1545–1568 (2017).
79. van Leeuwen, P. J. Particle filtering in geophysical systems. *Mon. Weather Rev.* **137**, 4089–4114 (2009).
80. Dubinkina, S., Goosse, H., Sallaz-Damaz, Y., Crespin, E. & Crucifix, M. Testing a particle filter to reconstruct climate changes over the past centuries. *Int. J. Bifurcat. Chaos* **21**, 3611–3618 (2011).

Acknowledgements

This research was funded by the ERC StG ICEPROXY project (203441), the ANR CLIMICE project, FP7 Past4Future project (243908), the RCN OCTEL project (248776/E10), the Belgian Research Action through Interdisciplinary Networks Mass2Ant project (BR/165/A2/Mass2Ant), the JSPS KAKENHI (grants 23244102 and 17H06318), the Royal Society Te Apārangi Marsden Fund (MFP-VUW1808) and the MBIE NZ Antarctic Science Platform (ANTA1801). It also benefited from the ESF PolarClimate HOLOCLIP project. D.S. benefited from the Blue-Action project (European Union's Horizon 2020 Research and Innovation Program, grant number: 727852) and the French LEFE-IMAGO programme. Hole U1357B samples and data were provided by the International Ocean Discovery Program (IODP).

Author contributions

X.C. designed and coordinated the study and led the writing. J.E. performed the HBI analysis on IODP Hole U1357B. P.C. and L.C.O. performed the diatom analyses on IODP

Hole U1357B and COR1GC cores, respectively. Q.D., H.G. and D.S. performed the data assimilation experiments. G.M., X.C. and A.M. coordinated the projects that funded the analyses. C.E., R.M.M. and R.B.D. performed the stratigraphic analysis of IODP Hole U1357B. M.I. gave access to COR1GC sediments and helped develop its age model. All authors commented on the manuscript and contributed to the writing.

Competing interests

The authors declare no competing interests.

Additional information

Extended data is available for this paper at https://doi.org/10.1038/s41561-021-00697-1.

Supplementary information The online version contains supplementary material available at https://doi.org/10.1038/s41561-021-00697-1.

Correspondence and requests for materials should be addressed to X.C.

Peer review information *Nature Geoscience* thanks the anonymous reviewers for their contribution to the peer review of this work. Primary Handling Editor: James Super.

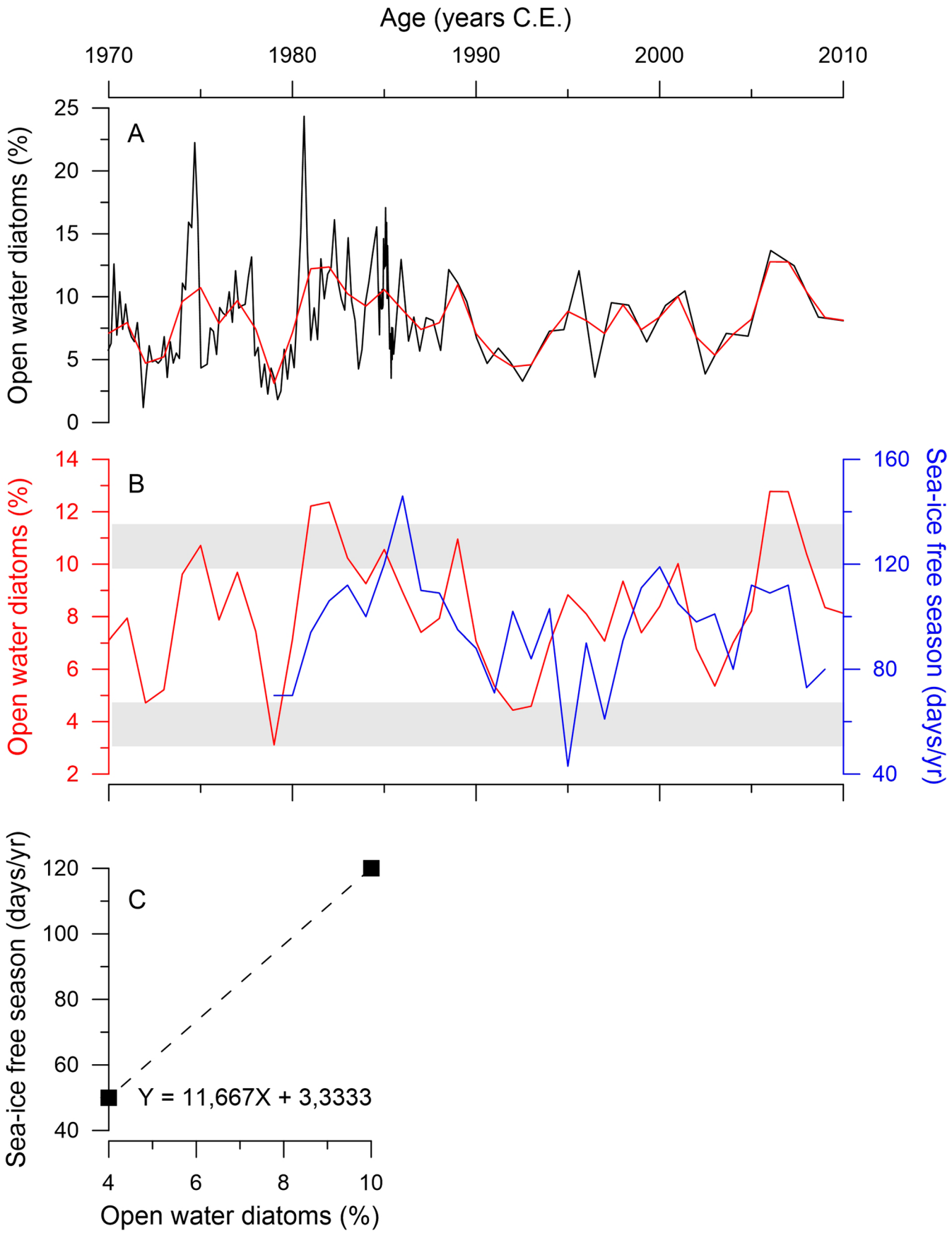

Extended Data Fig. 1 | See next page for caption.

Extended Data Fig. 1 | Scaling diatom relative abundances to sea-ice presence. a, Raw relative abundances of the Open Water Diatom (OWD) group in core DTCI2010 off Adélie Land (black line)[15] and resampled relative abundances of the OWD group at a 1 year resolution (red line). **b**, Resampled relative abundance of the OWD group at a 1 year resolution (red line) compared to the length of the yearly sea-ice free season off Adélie Land between 1979 and 2010 (blue line)[15]. Grey shaded boxes represent the upper and lower end members used to scale the relative abundances of the OWD group to the yearly open water length. **c**, The mean upper and lower end members used to calculate the equation to scale the OWD group relative abundances to the length of the open season.

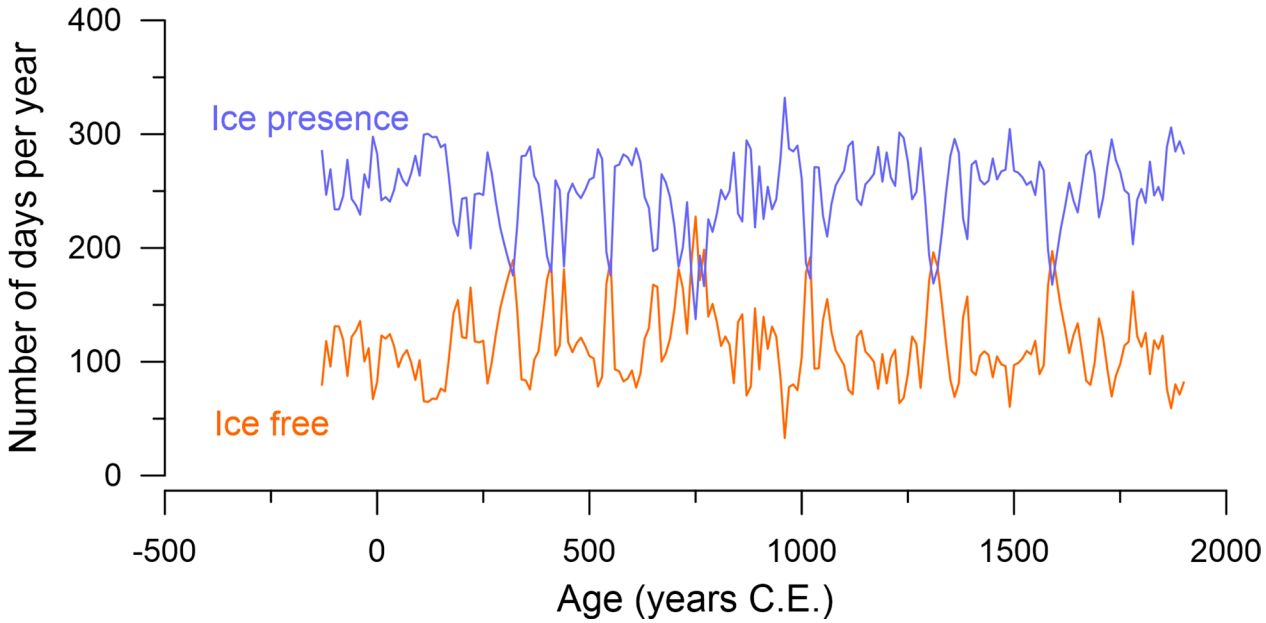

Extended Data Fig. 2 | Sea-ice duration off Adélie Land over the last 2000 years. Length of the sea-ice free season (orange line) calculated by applying the equation presented in Extended Data Fig. 1c to the relative abundances of the OWD group in IODP Hole U1357B and length of the sea-ice duration calculated (blue line) by subtracting the ice-free values from 365 days.